

We are IntechOpen, the world's leading publisher of Open Access books Built by scientists, for scientists

6,900

Open access books available

186,000

International authors and editors

200M

Downloads

Our authors are among the

154

Countries delivered to

TOP 1%

most cited scientists

12.2%

Contributors from top 500 universities



WEB OF SCIENCE™

Selection of our books indexed in the Book Citation Index
in Web of Science™ Core Collection (BKCI)

Interested in publishing with us?
Contact book.department@intechopen.com

Numbers displayed above are based on latest data collected.
For more information visit www.intechopen.com



Electrical Resistivity of Powdered Porous Compacts

Juan Manuel Montes, Francisco Gómez Cuevas,
Jesús Cintas, Fátima Ternero and
Eduardo Sánchez Caballero

Additional information is available at the end of the chapter

<http://dx.doi.org/10.5772/intechopen.76159>

Abstract

In this chapter, the problem of the electrical conduction in powdered systems is analyzed. New equations for computing the effective electrical resistivity of metallic powder aggregates and sintered compacts are proposed. In both cases, the effective electrical resistivity is a function of the bulk material resistivity, the sample porosity and the tap porosity of the starting powder. Additional parameters are required to describe the case of non-sintered powder aggregates: one of them describes a certain residual resistivity and another describes the rate of mechanical descaling during compression of the oxide layers covering the particles. Laws for the thermal dependence of these two parameters are also suggested. These new equations modeling the effective electrical resistivity are valid in all the physical range of porosity: from zero porosity to the tap porosity. Links between the proposed equations and the percolation conduction theory are stated. The proposed equations have been experimentally validated with powder aggregates (both in as-received state and after electrical activation to eliminate oxide layers) and sintered compacts of different metallic powders, resulting in a very good agreement with theoretical predictions. In addition to their general interest, the proposed models can be of great interest in modeling electrical consolidation techniques.

Keywords: electrical resistivity, powder metallurgy, modeling, effective properties, electrical consolidation techniques, FAST

1. Introduction

The theoretical prediction of the effective (or apparent) properties of heterogeneous materials (including multiphase materials, composites, porous materials, etc.) has a remarkable history, on times stimulating the interest of some eminent scientists, including Maxwell, Rayleigh and

Einstein, among others. In 1873, Maxwell derived an expression for the effective resistivity of a dispersion of spheres within a different material, although only accurate for dilute sphere concentration [1]. In 1892, Rayleigh developed a method to calculate the effective resistivity of an otherwise uniform material interrupted by a rectangular arrangement of spheres of different nature, which is still useful today [2]. In 1906, Einstein determined the effective viscosity of a diluted suspension of spheres, in a work which began the way to model the effective properties of heterogeneous materials [3]. From those first works until today, there has been an upsurge in the number of works dealing with this subject, not only because of the extraordinary intellectual challenge that they represent but also because of their undoubted technological interest.

Porous materials are a good example of heterogeneous materials of technological interest, and we will focus this work on them. Porous materials can be considered as two-phase materials: a phase consisting of the bulk material (fully dense material) and the other constituted by pores.

But, how to model the properties of heterogeneous materials? It is tempting to use 'mixture rules', with the appropriate weighting factors. In the case of porous materials, these rules result in particularly simple expressions, since the properties of one of the phases (the pores) are usually zero. In this way, in order to know the effective properties of porous materials, it would be sufficient to know the properties of the bulk material and the degree of porosity of the sample under consideration. However, for some properties, especially those related to transport phenomena, the aforementioned approach is not sufficient; other factors such as the average size of the pores, their size distribution, etc. are particularly important.

Even the indicated details are not sufficient when the porous materials are made of metallic powders (i.e. the powder metallurgy field). If this is the case, other details must be considered: the material may be the result of cold compacting a mass of powders or the result of compacting and then sintering in a furnace. There are more than mechanical differences between these two situations. From an electrical point of view, for example, in the first situation, metal-metal contacts between particles are not guaranteed. However, in the second case, the sintering process guarantees the electrical continuity (metal-metal contacts) in all the particle junctions. For this reason, the designation of 'porous materials' is too ambiguous. However, with 'powdered porous compacts', we refer to compacted powder aggregates or sintered compacts. Other authors prefer the expression 'granular materials' to refer to the same idea.

Regarding sintered materials, some expressions proposed for generic porous materials may be applicable. **Table 1** shows some of the reported expressions to model the effective electrical resistivity of porous media, obtained by theoretical, empirical or semiempirical means. The expressions in **Table 1** refer to relative (or normalized) resistivity, i.e. the ratio between the effective resistivity of the porous material and the resistivity of the bulk material ($\rho_R = \rho_E/\rho_0$). Some of them were proposed to describe thermal resistivity, but the problem is quite similar (although the transport mechanisms are not exactly the same.)

As can be seen in **Table 1**, most expressions include an empirical parameter. Resistivity is closely dependent on the microstructure (including pore shape and size), and this empirical parameter helps to model the effect of these details. Therefore, a simple mathematical expression based solely on the porosity degree, without any additional empirical parameter, can never accurately describe the electrical resistivity.

Authors	Year	Relative resistivity ($\rho_R = \rho_E / \rho_0$)	Upper boundary condition $\rho_R \rightarrow 1...$	Lower boundary condition $\rho_R \rightarrow \infty...$
Maxwell [1]	1873	$\frac{2+\Theta}{2(1-\Theta)}$	$\Theta \rightarrow 0$	$\Theta \rightarrow 1$
Fricke [4]	1924	$\frac{1+c_1\Theta}{1-\Theta}$	$\Theta \rightarrow 0$	$\Theta \rightarrow 1$
Loeb [5]	1954	$(1 - c_2\Theta)^{-1}$	$\Theta \rightarrow 0$	$\Theta \rightarrow 1/c_2$
Murabayashi et al. [6]	1969	$\frac{2+\Theta}{3(1-\Theta)^3 - (1-\Theta)}$	$\Theta \rightarrow 0$	$\Theta \rightarrow 1$
Aivazov et al. [7]	1971	$\frac{1+c_4\Theta^2}{1-\Theta}$	$\Theta \rightarrow 0$	$\Theta \rightarrow 1$
Meyer [8]	1972	$\frac{c_5+\Theta}{c_5(1-\Theta)}$	$\Theta \rightarrow 0$	$\Theta \rightarrow 1$
Schulz [9]	1981	$(1 - \Theta)^{-c_6}$	$\Theta \rightarrow 0$	$\Theta \rightarrow 1$
McLachlan [10]	1986	$\left(1 - \frac{\Theta}{\Theta_c}\right)^{-\frac{3}{2}\Theta_c}$	$\Theta \rightarrow 0$	$\Theta \rightarrow \Theta_c$
Montes et al. [11]	2003	$\left(1 - \frac{\Theta}{\Theta_M}\right)^{-2}$	$\Theta \rightarrow 0$	$\Theta \rightarrow \Theta_M$
Montes et al. [12]	2008	$\left(1 - \frac{\Theta}{\Theta_M}\right)^{-u}$ $u = 1 + (1 - \Theta_M)^{\frac{4}{3}}$	$\Theta \rightarrow 0$	$\Theta \rightarrow \Theta_M$
Montes et al. [13]	2016	$\left(1 - \frac{\Theta}{\Theta_M}\right)^{-\frac{3}{2}}$	$\Theta \rightarrow 0$	$\Theta \rightarrow \Theta_M$

The parameters c_1 to c_6 are material constants, Θ_c is a critical porosity (related to the percolation threshold) and Θ_M is the tap porosity of the starting powder (later described)

Table 1. Several expressions for the relative resistivity as a function of the porosity degree (Θ).

Naturally, the resistivity must increase with the porosity. The greater the porosity, the smaller the electric flow transfer section and the longer the path it must travel, contouring the pores. Most of the expressions in **Table 1** verify that relative resistivity increases from 1 to infinity as porosity varies from 0 to 1. However, this does not apply to powdered materials, as their maximum porosity is always lower than 1. Only the expressions of Loeb [5], McLachlan [10] and Montes et al. [11–13] take this into account, being even applicable in the range of high porosities.

Regarding powder aggregates under compression, modeling is always more difficult. The electrical resistance of the powder mass logically depends on its porosity, decreasing by increasing pressure. So, the bigger the pressure, the lesser is the porosity and therefore the lower is the electrical resistance. But pressure not only helps to reduce the porosity but also, due to the friction between particles, can force the descaling of the dielectric layers (mainly oxides but also hydrides and other chemical compounds) that normally cover the powder metallic particles. Both phenomena lead to decrease the effective resistivity of the powder mass by increasing pressure. These oxides have a high influence on the apparent value of the electrical resistance, to the point that may have more influence than the porosity itself. The influence of oxide layers (with a dielectric behavior) is crucial, since, despite their small thickness, they dramatically influence the conduction process. Some interesting experimental studies, focused on the electrical behavior, have helped to identify the complexity of the phenomena involved [14–16]. Some theoretical studies carried out by Montes et al. [13] have

attempted to identify the most relevant parameters of the problem, ensuring the applicability of the proposed expressions throughout the physical range of porosity and trying to maintain a minimum level of mathematical complexity. The proposed models incorporate parameters as the porosity of the sample, the initial porosity of the starting powder (tap porosity), the resistivity of the metal and the thickness and resistivity of the oxide layers. However, the models also need to incorporate two empirical parameters to describe the mechanical descaling of the oxide layers during the compaction process.

In this chapter, two new models to compute the effective electrical resistivity of metal powder systems under pressure (constituted by oxide-free metallic particles or by oxide-coated metallic particles) will be developed. These models can be considered valid for describing the electrical behavior both of sintered compacts and of powder aggregates, which will be tested to validate the proposed models. The new expressions will be useful to model the electrical consolidation techniques of metallic powders, which are commonly known as field-assisted sintering techniques (FAST).

2. Modeling of the effective resistivity

2.1. Effective areas and effective paths

Let us consider two cylindrical samples of the same material and equal dimensions, the first one being completely solid and the second one with a porosity Θ , as illustrated in **Figure 1**.

As a consequence of the porosity, the electrical resistance cannot be the same in the second sample. The electrical resistance (R) of a bulk material can be calculated from its resistivity. So, for a specimen with nominal section S_N and uniform nominal height of length L_N , the electrical resistance is

$$R = \rho_0 \frac{L_N}{S_N} \quad (1)$$

with ρ_0 being the resistivity of the bulk material.

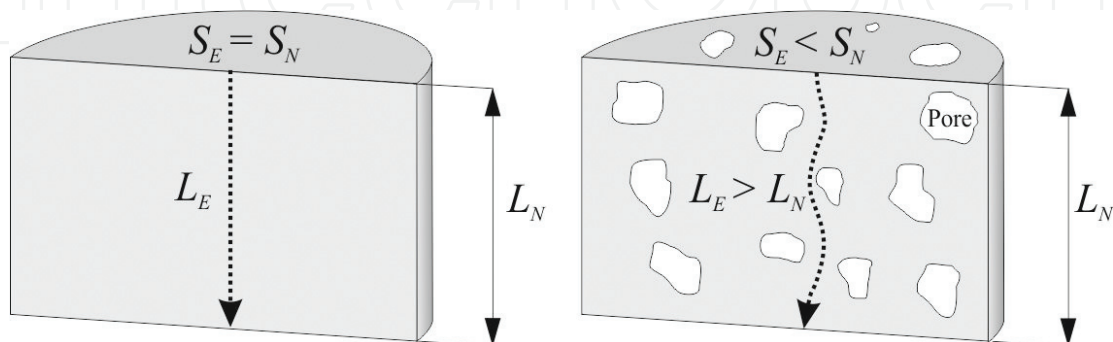


Figure 1. Diametrical cross sections of two cylindrical samples. Obviously, in the porous material, the electric flow path will be longer and more tortuous, while the transfer cross section will be smaller.

For the porous specimen, which may be produced by uniaxial press and sintering of metallic oxide-free powders, the resistance R' (higher than the one of the bulk specimen) can be calculated in two different ways. On the one hand, it may be considered that the porous material behaves as having an effective electrical resistivity, ρ_E , upper than ρ_0 , and this is

$$R' = \rho_E \frac{L_N}{S_N} \quad (2)$$

On the other hand, assuming that the resistivity of the porous material is equal to ρ_0 , the effective section for the electrical flow to pass, as well as the path length that the flow has to travel, must be different. Being S_E and L_E the effective values of, respectively, the mean transfer section (smaller than the nominal) and mean effective path (longer than the one corresponding to a bulk specimen), the resistance of the porous specimen could be expressed as

$$R' = \rho_0 \frac{L_E}{S_E} \quad (3)$$

It is possible to express S_E and L_E as functions of the specimen porosity (Θ). Thus, by equalling Eq. (2) and Eq. (3), it would be possible to obtain an expression for the effective resistivity, ρ_E , as a function of ρ_0 and the porosity degree. The problem is knowing how the effective magnitudes, S_E and L_E , depend on the porosity. A simple reasoning provides the solution. Let us assume that the porosity of the second specimen in **Figure 1** is completely removed by concentrating the material toward the inside, by decreasing its diameter, as is illustrated in **Figure 2**. The result will be a new, fully dense cylinder of the same height (L_N), cross-sectional area S_E and volume $V_{fully\ dense} = S_E \cdot L_N$.

According to the definition of porosity

$$\Theta = \frac{V_{void}}{V_{total}} = \frac{V_N - V_{fully\ dense}}{V_N} = 1 - \frac{V_{fully\ dense}}{V_N} = 1 - \frac{S_E \cdot L_N}{S_N \cdot L_N} = 1 - \frac{S_E}{S_N} \quad (4)$$

and therefore

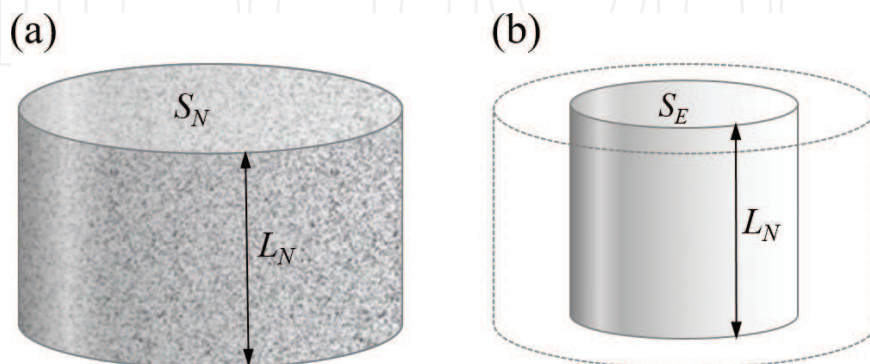


Figure 2. Initial porous sample and final sample obtained by concentrating all the material and preserving the same nominal height.

$$S_E = S_N(1 - \Theta) \quad (5)$$

This expression is well known in *stereology* and widely used in *quantitative metallography*. As can be checked, $S_E \rightarrow S_N$ as $\Theta \rightarrow 0$ (fully dense material) and $S_E \rightarrow 0$ as $\Theta \rightarrow 1$.

In order to model the mean effective path through a porous specimen, i.e. the distance to travel, eluding pores, from the top to the bottom of the cylinder, a similar expression can be stated. However, two considerations have to be taken into account: (i) we are now dealing with a distance instead of an area; therefore, the factor depending on the porosity should be $(1 - \Theta)^{1/2}$, and (ii) the other way round as with the effective area, the effective length increases with the porosity, and, thus, the relationship should be now inversely proportional.

It is then proposed as follows:

$$L_E = L_N(1 - \Theta)^{-1/2} \quad (6)$$

As can be checked, $L_E \rightarrow L_N$ as $\Theta \rightarrow 0$, but $L_E \rightarrow \infty$ as $\Theta \rightarrow 1$, being equivalent to say that there is not a continuous path.

However, for the description of powdered systems, the previous expressions of S_E and L_E require to be revised. There are also two situations to be distinguished: powder systems with oxide-free particles and powder systems with oxide-coated particles.

2.2. Resistivity of powder systems consisting of oxide-free particles

Until now, we have assumed the porosity to be uniformly distributed and to range from 0 to 1. We shall refer to systems fulfilling these two conditions as *foamed* porous systems, although the limit of $\Theta = 1$ could actually never be reached. The case of systems obtained from powders is far from fulfilling the above-mentioned limits. Theoretically, a sintered compact can be expected to reach a zero porosity upon sintering. However, the upper limit of porosity will never be reached. The maximum porosity in those systems, Θ_M , is the maximum undistorted equilibrium porosity. Essentially, this porosity is equivalent to the tap porosity, i.e. the porosity of a powder mass after being vibrated [17]. This latter parameter describes the pore structure and is very dependent on particle shape, size and distribution, in some way agglutinating morphometric information about the powder. We shall refer to systems satisfying this description as *powdered porous systems*. This entails altering Eq. (5) and Eq. (6) in order to include this upper bound for porosity. The required change is fairly simple and involves replacing the *porosity* (Θ) with the *normalized or relative porosity* ($\Theta_R = \Theta/\Theta_M$). Thus

$$S_E = S_N(1 - \Theta/\Theta_M) \quad (7)$$

Now, $S_E \rightarrow S_N$ as $\Theta \rightarrow 0$, as in the fully dense material, but in the upper porosity bound, $S_E \rightarrow 0$ as $\Theta \rightarrow \Theta_M$, situation where interparticle contacts in the powder are points. S_E represents the effective section for the electrical current transfer, and being this section null, the transfer is not possible.

A similar expression can be stated to model the mean effective path. It is then proposed as follows:

$$L_E = L_N(1 - \Theta/\Theta_M)^{-\frac{1}{2}} \quad (8)$$

As can be checked, $L_E \rightarrow L_N$ as $\Theta \rightarrow 0$, but $L_E \rightarrow \infty$ as $\Theta \rightarrow \Theta_M$, being equivalent to say that there is no continuous path in the non-pressed system.

In previous works, Montes et al. proposed the same theoretical expression for the effective transfer section [18–20] but a different expression for the effective path [21]. The difference is not so large and can be absorbed by very small differences in the values of Θ_M , which cannot be empirically discerned due to the experimental uncertainty.

By substituting Eq. (7) and Eq. (8) into Eq. (3), the expression below is obtained:

$$R' = \rho_0 \frac{L_N}{S_N} (1 - \Theta/\Theta_M)^{-\frac{3}{2}} \quad (9)$$

Equalling Eqs. (2) and (9), the next final expression is obtained:

$$\rho_E = \rho_0 (1 - \Theta/\Theta_M)^{-\frac{3}{2}} \quad (10)$$

Eq. (10) satisfies the expected boundary conditions, $\rho_E \rightarrow \rho_0$ as $\Theta \rightarrow 0$ and $\rho_E \rightarrow \infty$ as $\Theta \rightarrow \Theta_M$ since, in this last situation, interparticle contacts are points.

It is interesting to compare Eq. (10) with the previously proposed expressions (see **Table 1**). As the exponent 2 in [11] resulted to be too high, when fitting the expression to experimental data, authors were forced to introduce a correction in the value of Θ_M , moving it away from the experimentally measured value. Regarding the expression proposed in [12], the exponent u takes different values depending on the value of Θ_M . For instance, and considering extreme values, for $\Theta_M = 0.35$, $u = 1.71$, whereas for $\Theta_M = 0.65$, $u = 1.43$. Both 1.71 and 1.43 can be approximated to 1.5. This is supported by the experimental uncertainty in the determination of the Θ_M value. Therefore, as compared with the expression derived in [12], the expression now proposed can be seen as a convenient simplification. Eq. (10) was also derived in [13] following a similar but different approach.

2.3. Resistivity of powder systems consisting of oxide-coated particles

An important detail that must be included to model oxidized powder aggregates is the fact that the oxide films coating the particles are altered throughout the compression process. During the early instants of compression, shear occurs along particle contacts because of sliding [22]. As a consequence of this shear, oxide films locally break, allowing the formation of metal–metal electric paths with rather lower electric resistance [14, 15]. This descaling effect that occurs during particle rearrangement is sufficiently important to be taken into account.

In view of Eq. (10), we can propose a similar expression to model the new situation:

$$\rho_E = \rho_{res} (1 - \Theta/\Theta_M)^{-n} \quad (11)$$

where ρ_{res} is the residual resistivity (higher than or equal to ρ_0) that would remain at $\Theta = 0$, as a consequence of the mechanical descaling process not being completed. Only if the oxide layers descaling during compression is complete, $\rho_{res} = \rho_0$ (actually, this limit value does not correspond to that of the bulk material, because the oxide layers, once removed, remain in the material and, although representing a very small volume fraction, slightly alter the resistivity value). The exponent n is a fitting parameter, which describes the descaling rate; if there are no oxide layers, its value would be equal to $3/2$, but with their presence it will take higher values.

Thus, for $\Theta \rightarrow \Theta_M$

$$\lim_{\Theta \rightarrow \Theta_M} \rho_E = \rho_{res} \cdot (1 - 1)^{-n} = \rho_{res} \cdot (\infty) = \infty \quad (12)$$

On the other hand, in the limit that $\Theta \rightarrow 0$

$$\lim_{\Theta \rightarrow 0} \rho_E = \rho_{res} \cdot (1 - 0)^{-n} = \rho_{res} \quad (13)$$

Comparing Eq. (11) with Eq. (10), it follows that the minimum value of the exponent n must be $3/2$. When the oxide dielectric layers are very thick and/or very resistive, the value of the resistivity during the first moments of compaction will be much higher than with bare particles, and the descaling effect will be very pronounced. Then, the exponent n will take values greater than $3/2$.

2.4. Percolation theory relationship

Eqs. (10) and (11) are similar to that derived from the percolation theory [23–26]. In fact, a simple algebraic manipulation of Eq. (10) leads to

$$\rho_E = \rho_0 (1 - \Theta/\Theta_M)^{-\frac{3}{2}} = \rho_0 \left(\frac{\Theta_M - \Theta}{\Theta_M} \right)^{-\frac{3}{2}} = \rho_0 \left(\frac{1 - \Theta - 1 + \Theta_M}{\Theta_M} \right)^{-\frac{3}{2}} \quad (14)$$

and, as the term $(1 - \Theta)$ coincides with the relative density ϕ , by defining the relative tap density $\phi_c = (1 - \Theta_M)$, it is obtained that

$$\rho_E = \rho_0 \left(\frac{\phi - \phi_c}{1 - \phi_c} \right)^{-\frac{3}{2}} \quad (15)$$

where the denominator is a constant, so it follows that

$$\rho_E \propto (\phi - \phi_c)^{-\frac{3}{2}} \quad (16)$$

which is what the percolation theory predicts [23–26], if admitted that ϕ_c , obtained from the tap porosity (Θ_M), represents the percolation bound and $3/2$ is the percolation exponent.

A similar reasoning can be applied to Eq. (11), leading to the same conclusion.

2.5. Model comparison

It is instructive to compare the theoretical predictions resulting from Eq. (10) and Eq. (11). Two systems will be considered. The first one is a powder mass with bare particles (applicable to sintered compacts or pressed compacts of deoxidized particles). The second one is a powder mass with particles coated by native oxides (oxidized particles). According to the considered equations, the relative electrical resistivity for both powder masses under compression varies with the porosity degree as shown in **Figure 3**.

As shown, the variation by increasing pressure of both curves starts at the same porosity value (the tap porosity), but the shape is not the same, due to the effect of the oxide descaling.

2.6. Influence of temperature

Although the resistivity of metals increases linearly with temperature, the resistivity of oxide layers decreases with temperature and in a more drastic way, which is usually described by means of an exponential law [27]:

$$\rho_x(T) = A_x \exp(E_x / (2k_B T)) \quad (17)$$

where A_x is a pre-exponential factor, E_x is the band-gap energy and k_B is the Boltzmann constant. So, for sufficiently high temperatures ($T \rightarrow \infty$), the resistivity of the dielectric or semiconductor layers will be significantly reduced. Dielectric breakdown of the layers may also occur. (Note that the expression $E_x / (2k_B)$ must have temperature dimensions.)

Taking into account this expression, it seems sensible to assume a similar behavior for ρ_{res} and the exponent n in Eq. (11), which should vary with temperature as follows:

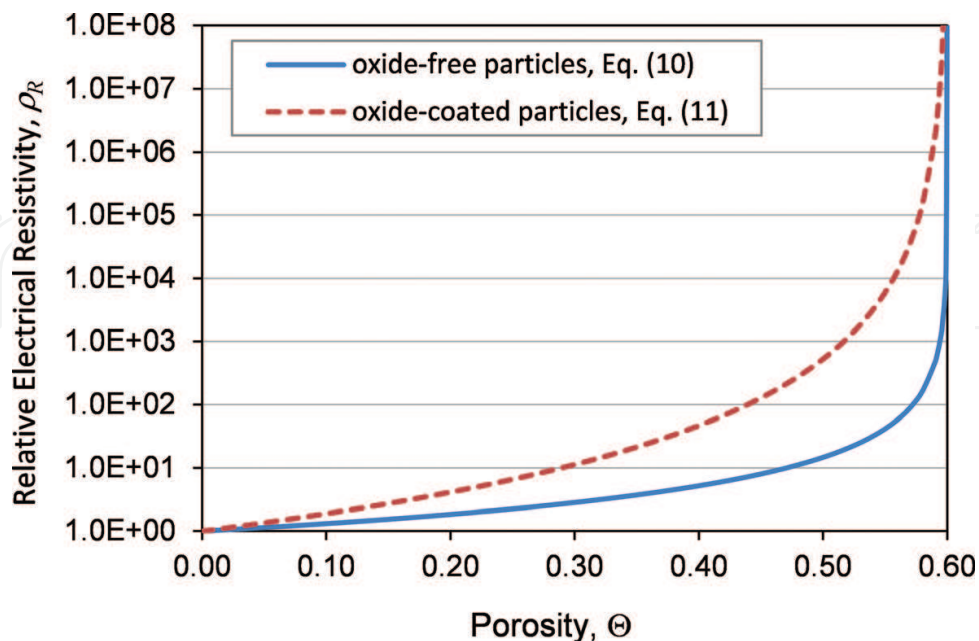


Figure 3. Relative electrical resistivity (ρ_E / ρ_0 or ρ_E / ρ_{res}) vs. porosity for a powder mass of oxide-free particles (solid line) and oxide-coated particles (dashed line). Curves have been computed by considering the arbitrary values $\Theta_M = 0.6$ and $n = 7/2$.

$$n(T) = \frac{3}{2} \exp(T_n/T) \quad (18)$$

$$\rho_{res}(T) = \rho_0 \exp(T_\rho/T) \quad (19)$$

where T_n and T_ρ are two convenient temperatures related to the corresponding activation energies.

Thus, as $T \rightarrow \infty$, $n \rightarrow 3/2$, which is the value that the exponent n takes for oxide-free particles (see Eq. (10)), i.e. without dielectric layer coatings. Similarly, as $T \rightarrow \infty$, $\rho_{res} \rightarrow \rho_0$, i.e. the resistivity of the metal, which means that the oxide effect is zero, as if they were not present.

The electrical resistivity values of the oxide films coating the powder particles are difficult to find. The chemical and physical nature of this oxide film cannot be accurately known in most cases. Moreover, the oxide film may contain metal atoms in various oxidation states, and the oxides may be accompanied by some hydroxides. Moreover, thin oxide films covering particles may behave in a rather different way of bulk oxides. The small thickness of the oxide layer alters the resistivity value by diminishing it, according to the Fuchs-Sondheimer law [27]. It is then concluded that it is difficult to know the exact nature and electrical resistivity of the oxide layers. We also ignore the relationship between T_n or T_ρ and E_x .

Fortunately, it is possible to calculate the values of T_n and T_ρ from Eq. (17) and (18), once the values of n and ρ_{res} are known at room temperature. By isolating n and ρ_{res} from the above equations, we obtain

$$T_n = T \cdot \ln(2n/3) \quad (20)$$

$$T_\rho = T \cdot \ln(\rho_{res}/\rho_0) \quad (21)$$

2.7. Connection with the applied pressure

Eqs. (10) and (11) relate the effective electrical resistivity of the powder aggregate to its porosity. Alternately, it would be possible to take into account the relationship between the electrical resistivity and the applied pressure, as has been done by other authors [28]. However, the fact that Eq. (10) and Eq. (11) are formally equal is a great success of the porosity-based description. The pressure-based description appears to have a narrower applicability, because although sintered compacts are in general previously subjected to compression, there is the possibility of obtaining very porous materials (with metal-metal contacts) without applying pressure, due only to the heat effect, as is the case in loose sintering. In such scenario, it is possible to consider a 'pressure' equal to the driving force that causes the decrease of energy per unit of volume (J/m^3 is equivalent to Pa), but this interpretation seems somewhat tortuous and impractical. Therefore, the description based on the porosity appears to have a wider applicability than that based on the applied pressure.

There is also a technical reason for preferring a porosity-based description. Although during the determination of the resistivity-porosity curve, it is also possible to record the applied pressure, and the punches (made of electrolytic copper) limit the value of the highest attainable pressure.

However, it is perfectly possible to make a compressibility curve of the powders reaching very high-pressure values, by using hardened steel punches (The compressibility curve collects information of how the porosity (or relative density) of the powder mass varies when it is subjected to an increasing compression.). Thus, the porosity-based description can be supplemented by an analytical description of the compressibility curve of the powder. Once the corresponding compressibility curve is obtained (Θ vs. P_N), it can be fitted by the least squares method to the analytical expression, for example, the one proposed by Secondi [29], which can be expressed in porosity terms as

$$\Theta = \Theta_{\infty} + (\Theta_M - \Theta_{\infty})\exp\left(- (P_N/a)^b\right) \quad (22)$$

where Θ is the porosity of the powder mass under a compacting pressure P_N . The parameter Θ_M is again the tap porosity of the powder. The other parameters (Θ_{∞} , a and b) are fitting parameters.

Therefore, on the one hand, Eqs. (10) and (11) relate ρ_E to Θ , and on the other hand, Eq. (21) relates Θ to P_N . Considering both equations, it is possible to relate ρ_E to P_N , which may be helpful for some situations.

3. Experimental validation

3.1. Materials

To validate Eqs. (10) and (11), four powders (three elemental and one alloy) with different nature, granulometry and tap porosity were chosen. The choice was guided by the intention of checking whether the parameter Θ_M used in the models allows for bringing out these differences.

Table 2 lists the commercial designation of each powder, the designation used here, the mean particle size obtained by laser diffraction and the tap porosity (Θ_M) measured according to MPIF Standards [17]. **Figure 4** shows SEM images with the different powders shape.

The absolute error during the measurement of the Θ_M value, as a function of the employed instrument precision, results to be ± 0.01 : a very small value as compared to the measurements. However, the random vibration process during measuring can lead to an increase of the experimental uncertainty. Experimental checks confirm a higher value around ± 0.05 , which is still a relatively small value.

Powder	Designation	Mean size (μm)	Θ_M (measured)
AS61 aluminum (Eckart-Werke)	Al	77.0	0.45
89/11 AK bronze (Eckart-Werke)	Bz	57.2	0.43
WPL 200 iron (QMP)	Fe	84.4	0.63
T255 nickel (Inco)	Ni	18.8	0.86

Table 2. Mean particle size and measured tap porosity (Θ_M) of tested powders.

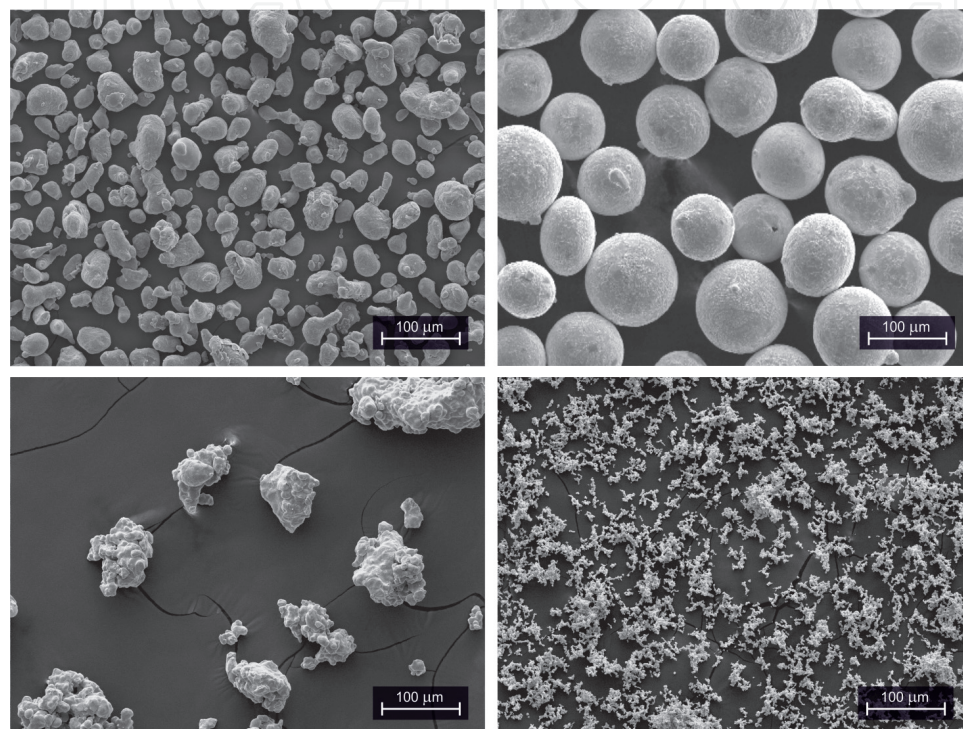


Figure 4. Scanning transmission microscopy (SEM) images of the four powders used for experimental validations. From left to right and top to bottom: Al, Bz, Fe and Ni.

3.2. Effective electrical resistivity of sintered compacts

There are two possible ways to validate Eq. (10). The first way consists in deoxidizing the powders and subjecting them to varying pressures to determine their resistivity, all under an inert atmosphere that guarantees the non-reoxidation of the particles. The second way consists in pressing the as-received powders (oxidized) to different pressures obtaining different compacts and, once compacted, carrying out a sintering process. This ensures that there are true metal–metal contacts between the particles. Due to the technical difficulties in the first option, the second one has been followed in this work.

Electrical resistance measurements were carried out by using a four-point probe and a Kelvin bridge (micro-ohmmeter), by performing two measurements with inverted polarities to minimize the parasitic effects. The electrical resistance was measured on cylindrical sintered compacts with different porosities. Resistivity was determined from the measured resistance value,

R_{mv} by applying the known expression $\rho_E = 2\pi sR_{mv}$, where $s = 2$ mm, is the distance between the probe electrodes.

These cylindrical samples (about 10 mm height, 12 mm diameter) were prepared by uniaxial cold compaction and subsequent sintering. Several compacting pressures were selected according to the compressibility curve to achieve the desired porosities, which ranged from the maximum allowing a handily specimen to the one obtained for a pressure of 1400 MPa. Afterwards, sintering was carried out for 30 minutes at the temperature indicated in **Table 3** under $1.2 \cdot 10^5$ Pa argon atmosphere. The final porosity after sintering (Θ) was again measured by weighting and measuring the specimens, and the resulting values, shown in **Table 3**, were used in the later calculations.

For comparison purposes, fully dense reference samples of each powder were produced by a double pressing at 1400 MPa (with intermediate annealing to a half of the sintering temperature) and final sintering during 3 hours. **Table 4** gathers the experimentally determined resistivity values of the fully dense samples, used like ρ_0 values. Also, included are the values of the bulk materials, at the measuring temperature ($\sim 25^\circ\text{C}$), found in the literature [30]. These later values are some lower, probably due to the presence in the fully dense samples of some residual porosity and the contamination introduced by the surface oxides of the powder particles.

The *porosity-effective resistivity* data cloud was then fitted to the expression of Eq. (10) by the least squares method. The only fitting parameter was Θ_M . The validity of the proposed model will be assessed depending on how the fitted Θ_M value compares to the experimental value gathered in **Table 2**.

Powder	Sintering temperature ($^\circ\text{C}$)	Porosity range
Al	650	0.01–0.32
Bz	850	0.05–0.10
Fe	1150	0.02–0.43
Ni	800	0.05–0.19

Table 3. Sintering temperature used to produce the tested specimens, previously pressed at different pressures, and porosity range attained.

Powder	Fully dense resistivity (ρ_0 [$\Omega\cdot\text{m}$])	Bulk material resistivity ($\Omega\cdot\text{m}$)
Al	2.922×10^{-8}	2.730×10^{-8}
Bz	1.862×10^{-7}	1.805×10^{-7}
Fe	1.177×10^{-7}	1.043×10^{-7}
Ni	8.197×10^{-8}	6.993×10^{-8}

Table 4. Electrical resistivity of fully dense parts and bulk materials, at room temperature.

Figure 5 shows the data clouds referred to the pairs (Θ, ρ_E) and (Θ_R, ρ_R) for each one of the tested powders. Also shown are the fitted theoretical curves, according to Eq. (10), which is only one when using relative variables. **Table 5** gathers the resulting values of Θ_M after fitting and the coefficients of determination, R^2 , obtained for each one of the powders.

As can be seen, the resulting fitting indicators are quite acceptable. Fitted Θ_M values are inside the accepted uncertainty range of ± 0.05 of the experimental values, except for the Ni powder. In this case, the fitted value (0.71) is far from the experimental one (0.86). This deviation could be due to the filamentary morphology of this powder and its great tendency to form agglomerates. This can distort the measurement of the tap porosity to a value higher than the actual value. A very small compression is sufficient for the porosity to decrease drastically to a value of about 0.7, which is the resultant value of the fitting process. Nevertheless, it seems that for this type of powder morphologies, the tap porosity does not result an adequate parameter.

It is interesting to compare the expression proposed in this chapter with the expressions suggested by other authors (**Table 1**). For this purpose, the experimental curve of the arbitrarily

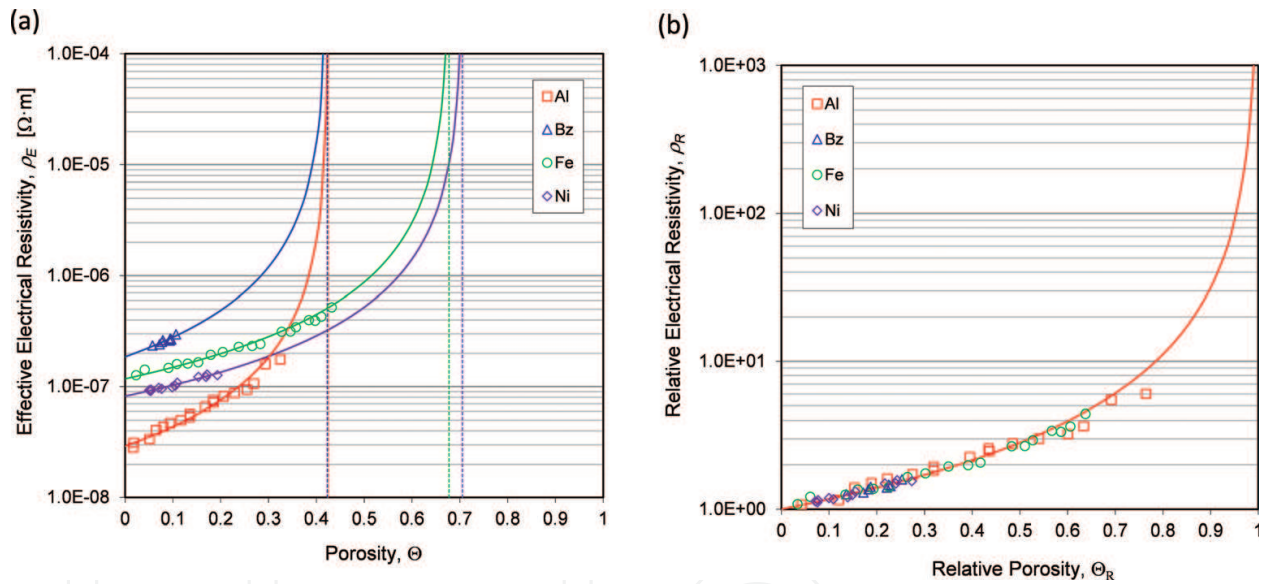


Figure 5. Experimental results (symbols) and fitted curves (lines) according to Eq. (10). (a) Effective electrical resistivity vs. porosity and (b) relative electrical resistivity (ρ_E/ρ_0) vs. relative porosity (Θ/Θ_M), for the different studied compacts. The vertical lines in (a) represent the fitted Θ_M values of the tested powders.

Powder	Θ_M (measured)	Θ_M (fitted)	R^2
Al	0.45	0.424	0.957
Bz	0.43	0.422	0.855
Fe	0.63	0.678	0.982
Ni	0.86	0.706	0.962

Table 5. Values of the adjustable parameter of Eq. (10), the tap porosity Θ_M and the resulting coefficients of determination after fitting to the experimental data.

chosen Fe compacts has been fitted with all the expressions (**Figure 6**). The value of ρ_0 has always been set equal to the value shown in **Table 4**, for the fully dense sample.

As can be seen, the expression proposed in this chapter offers one of the best coefficients of determination. For the first seven expressions, the fitting parameter does not have a clear physical meaning, so, nothing can be discussed in favor or against the obtained value. For the McLachlan expression [10], the obtained parameter c results are too low to be identified with the tap porosity. Similarly, for the expression reported by Montes et al. [11], c results are too high, even higher than the measured tap porosity. If the fitting process is forced in these two cases to make the parameter c to move in into admissible values (between 0.58 and 0.68), the coefficient of determination decreases to 0.8960 and 0.7647, respectively. Regarding the expression in [12], the obtained result is quite good, with a realistic value of the fitting parameter, and also with the expression proposed in this chapter, with the added advantage of a being a simpler expression.

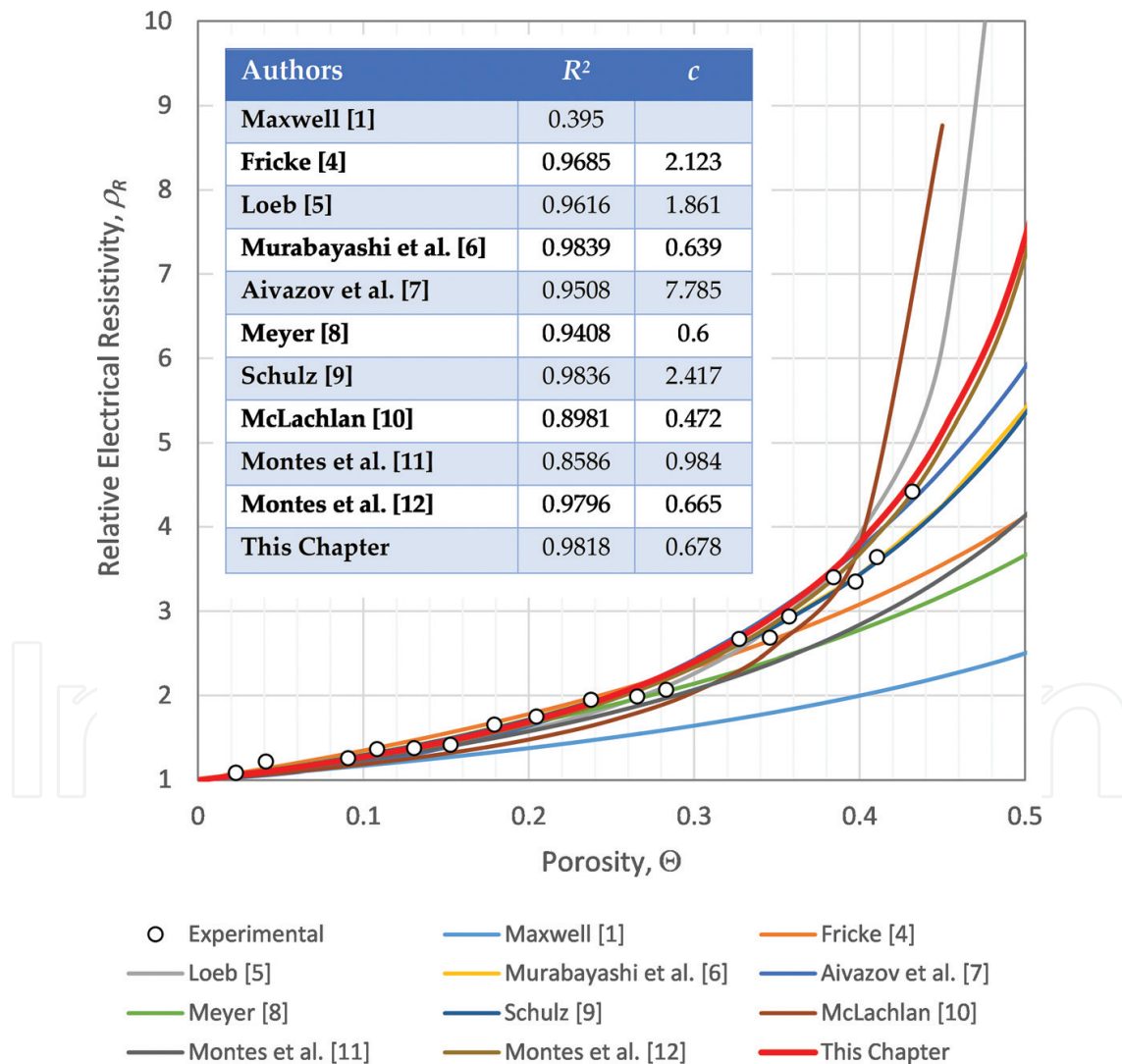


Figure 6. Curves resulting after fitting the experimental data of the Fe compacts with the different theoretical expressions gathered in **Table 1**. The value of ρ_0 was fixed to $1.177 \times 10^{-7} \Omega\cdot\text{m}$, corresponding to the fully dense sample. The inserted table shows the coefficient of determination and the fitting parameter, c , in each expression.

3.3. Effective electrical resistivity of powder aggregates

It is now the intention to validate Eq. (11) for oxidized powder aggregates. The measuring system consisted of a cylindrical die made of alumina (12 mm inner diameter and resistivity $\sim 10^{12} \Omega \cdot \text{m}$), with an external steel hoop to reinforce the brittle ceramic. Two electrodes (of electrolytic copper) closed the die, with the powder mass in the middle. The porosity of the powders was reduced by increasing the pressure and therefore moving the upper electrode (the lower one remained fixed). After pouring the powder into the die, it was vibrated according to the standards [17] in order to reach the tap porosity. The measuring process started soon after the upper punch touched the powders. At each step, the height of the powder column and its electrical resistance were recorded (the former through the displacement of the universal testing machine frame, and the latter through a micro- or kilo-ohmmeter connected to the electrodes). The load was increased to record a new point. For each measured resistance value (R), the effective resistivity value (ρ_E) can be calculated using the well-known formula $\rho_E = R \cdot S/H$, where S is the cross-sectional area and H is the height of the powder column. The porosity can also be easily computed from the powder column height.

The experimental results and fitted theoretical curves according to Eq. (11) are shown in **Figure 7**. Note that although for the representation in **Figure 7b** relative variables have been used, there is not a common theoretical equation for all the powders because the influence of the descaling process is different from each one. Fitted values of the adjustable parameters (Θ_M , ρ_{res} and n), as well as the coefficients of determination, R^2 , are gathered in **Table 6**. As can be seen, the results are quite consistent, with coefficients always greater than 0.99.

Now, in all cases, fitted Θ_M values are within the experimental uncertainty (about ± 0.05). The obtained value for Ni is interesting, now in a total agreement with the measured value despite the morphological characteristics of the powder have not changed. The presence of two other fitting parameters allows Θ_M reaching the objective value, which probably causes a slight

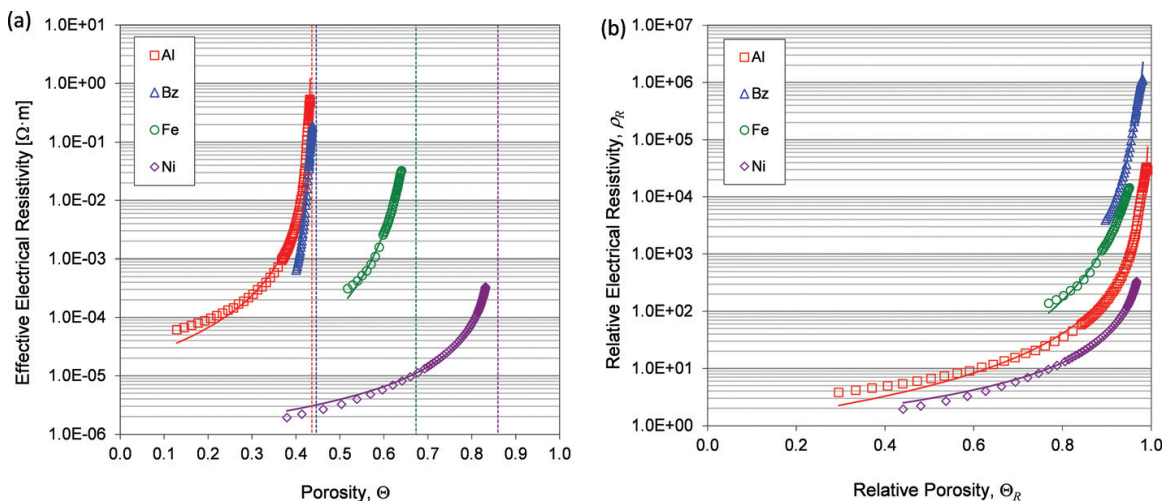


Figure 7. Experimental results (symbols) and fitted curves (lines) with Eq. (11) of (a) the effective electrical resistivity vs. porosity and (b) relative electrical resistivity (ρ_E/ρ_{res} with ρ_{res} taken from **Table 6**) vs. relative porosity (Θ/Θ_M), for the four studied powders. The vertical lines in (a) represent the fitted tap porosity values.

Powder	Θ_M (fitted)	ρ_{res}	n	R^2	Θ_M (measured)	ρ_x ($\Omega \cdot m$)
Al	0.436	1.618×10^{-5}	2.311	0.990	0.45	1.0×10^{12} [31]
Bz	0.446	1.880×10^{-7}	3.639	0.987	0.43	1.0×10^2 [32]
Fe	0.673	2.263×10^{-6}	3.200	0.998	0.63	2.1×10^3 [33]
Ni	0.860	1.000×10^{-6}	1.522	0.998	0.86	8.0×10^2 [34]

For comparison purposes, in the last two columns, the measured value of Θ_M and the oxide resistivity at room temperature, found in thin film-specialized literature, are shown

Table 6. Fitting parameter values and coefficient of determination for the studied powders.

alteration in the other parameters. Unfortunately, the filamentary morphology of the powder does not allow to be totally confident with the obtained results.

A detailed study of the fitted value of ρ_{res} and n is also worth performing. Regarding the value of ρ_{res} , and also considering the ρ_x value shown in **Table 6**, it can be said that there is a correlation between the two values: if the values of ρ_{res} and ρ_x are ranked from highest to lowest, the list obtained is the same. This is logical, considering that ρ_{res} is due to the remains of the oxide layers that have not been removed.

Obviously, the values of ρ_{res} cannot be lower than those of the bulk metal, ρ_0 , given in **Table 4**. As can be seen, all the values of ρ_{res} exceed in one or more orders of magnitude of the corresponding values of ρ_0 , with the exception of the bronze (Bz) whose ρ_{res} is only slightly higher than its respective value of ρ_0 . This very small difference means that the oxide can flake out completely or that the oxide layer is much thinner in this powder.

On the other hand, the results obtained for n are not so easy to interpret. Obviously, these have to do with the oxide descaling easiness. But the nature of this phenomenon is complex, depending on multiple factors: the shape, size and hardness of the particles, the thickness of the oxide layers, the mechanical strength and brittleness of these layers, etc. The difficulty to collect all this information aggravates the problem [35].

It is possible, however, as already mentioned, to calculate the values of the activation energies associated with the parameters n and ρ_{res} , present in Eq. (11). **Table 7** shows the resulting values after replacing in Eq. (19) and Eq. (20) in the values of n and ρ_{res} shown in **Table 6** for tests carried out at room temperature (298 K).

Powder	T_n (K)	T_p (K)
Al	128.846	1.88×10^3
Bz	264.095	2.87
Fe	225.792	8.81×10^2
Ni	4.334	7.45×10^2

Table 7. Activation energies associated with parameters n and ρ_{res} .

The relatively small differences in the n and ρ_{res} values shown in **Table 6** are now magnified. A clear difference is found among resulting values. Concerning T_n , the Ni powder shows a value of two orders of magnitude lower. This means that for temperatures not too high, the effect of the nickel oxide will not be much important. In the limit situation, with oxide-free particles, T_n takes the limit value 0 at any temperature. When the oxide is present, the value of T_n gives an idea of the effect of the oxide at the considered temperature. On the other hand, according to the T_p values, for temperatures not too high, the resistivity of the bronze oxide will be similar to that of the metal. The effect of the resistivity at different temperatures can be followed with the T_p value.

3.4. Model application

Up to now, the goodness of the developed relationships between electrical resistivity and porosity has been checked, both in oxide-free and oxide-covered particles. As a result, the fitting parameters of the model have been proven to agree with the expected ones or, in some cases, have just been determined to fit the experimental data. A step further in the applicability of the final model (considering the previously obtained fitting parameters) consists in comparing the predictions for new situations with the corresponding new experimental results, this time without free value parameters.

However, before undertaking this, there is still a pending issue, defining the relationship between ρ_E and P_N established in Eq. (21). The first step consists in subjecting the selected powders to compression tests, using a universal testing machine according to the standards [36]. **Figure 8** shows the obtained curves (in Θ vs. P_N representation) and the theoretical curves resulting from fitting by the least squares method the experimental curves to the Secondi expression. **Table 8** gathers the values of the parameters involved in Eq. (21) and the obtained determination coefficients.

There are not many comments to make about the results, because apart from Θ_M , the other parameters do not have a physical meaning. Regarding Θ_M , the fitted values are inside the uncertainty interval except for the Ni powder. In this case, the fitted value is again quite different to the experimentally measured, but being the same as the one obtained when also working with oxide-covered powders during checking of Eq. (11). The powder morphology accounts again for the observed difference.

Once the values of the parameters present in Eq. (10) and (21) are known, the predictability of the model can be checked. For this purpose, new electrical resistance measurements were made on the four powders under some different experimental conditions. An 8-mm-internal diameter die was used (instead of the one used to determine compressibility and compressibility/resistivity curves, with 12 mm). Measurements were made with three different masses, 6, 8 and 12 g and with four different pressures (25, 50, 75 and 100 MPa). The measured values of electrical resistance and the predicted values obtained using Eq. (10), Eq. (21) and the known expression $R = \rho_E H/S$ are shown in **Figure 9**, for the iron powder. As can be seen, the values differed by less than 2%, with an average relative error of 0.83%, which can be considered a reasonable agreement. For the remaining powders, similar results were obtained.

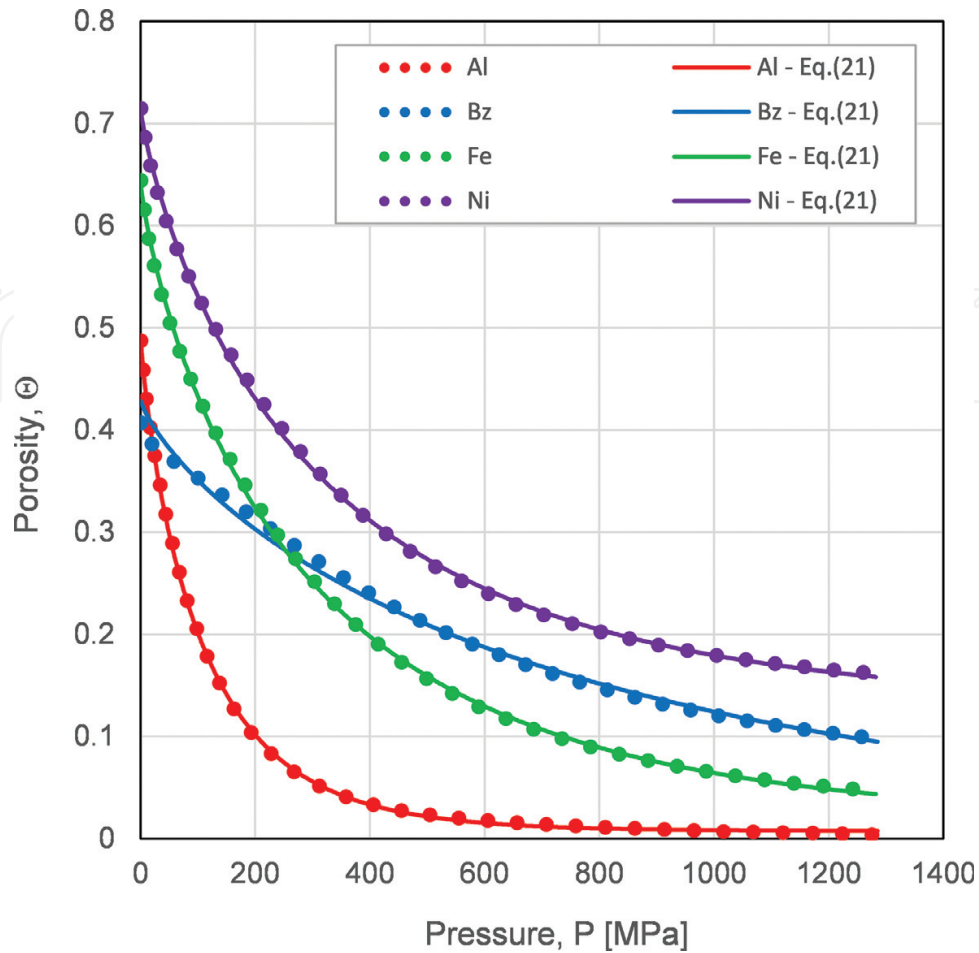


Figure 8. Experimental compressibility curves and corresponding fitted curves obtained by fitting by the least squares method the Secondi expression to the experimental data.

Powder	Θ_{∞}	Θ_M	a	b	R^2
Al	0.007	0.494	110.6680	0.8381	0.9998
Bz	0.000	0.430	759.5506	0.7865	0.9923
Fe	0.016	0.645	304.9329	0.7967	0.9997
Ni	0.130	0.716	329.6176	0.8132	0.9997

Table 8. Fitted values of the parameters involved in the Secondi expression (Eq. (21)).

3.5. Electrical activation

In some electrical consolidation techniques of powders, it is practical to incorporate an electrical activation stage, whose purpose is precisely to eliminate the insulating effect of the oxide layers by electrical means. It is possible to avoid the effect of these oxide layers by employing high or medium voltages (>200 V). High electrical currents are not necessary. During the first moments of the process, the interparticle contact areas are very small and therefore very resistive, and the local temperature of these areas can quickly and notably increase. This local

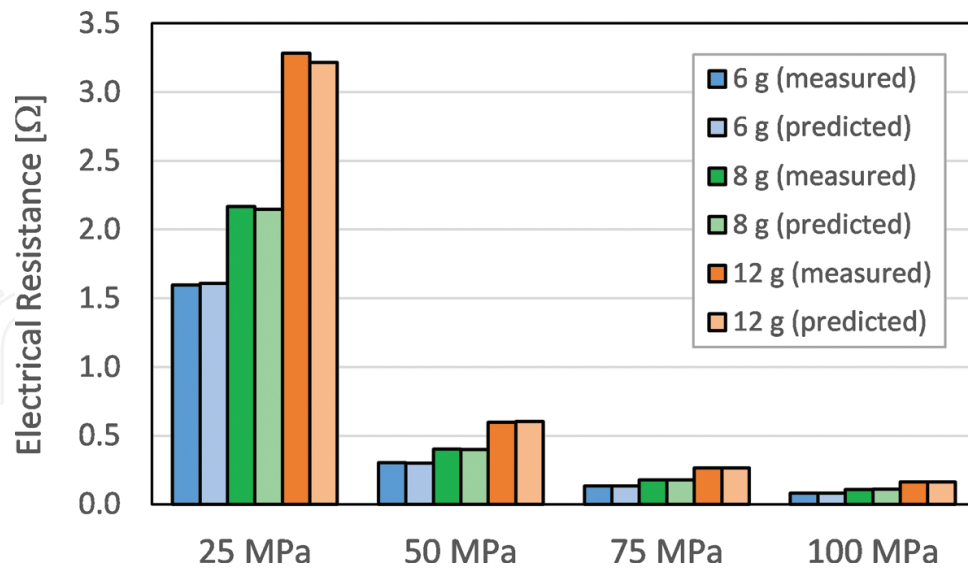


Figure 9. Measured and predicted resistance values for Fe powder columns under different pressures and masses.

temperature increment will result in a drastic decrease in the resistivity of the oxide layers, dielectric or semiconductor in nature. If the local temperature or applied electric fields become sufficiently high, the dielectric breakdown of these layers could also occur, often leading to an irreversible degradation.

In order to test both the model and the efficiency of the electrical activation process, the resistance measurements obtained after activating Fe powder columns (under the same aforementioned conditions), and the predicted values through the model of oxide-free particles given by Eq. (10), are compared. The electrical discharge came from an autotransformer capable of providing a voltage of 0–220 V and a maximum current of 10 A, protected by a magnetothermic circuit breaker. The voltage was slowly increased until the circuit breaker opened the circuit. Then, resistance measurements were carried out. **Figure 10** shows the measured electrical resistance values, as well as the predicted ones. In this case, the maximum relative error is 9.5%, with seven of the experiments having an error greater than 5%, and with an average relative error of 4.9%.

It is worth noting that the resistance values shown in **Figure 9** are three orders of magnitude higher than those shown in **Figure 10**. The higher values must be due to the presence of oxide layers, only partially peeled by pressure, and to their absence (partial or total) in the second case. After the application of the electrical activation, resistivity decreases as a consequence of the temperature increase or the degradation of the dielectric layers. The observed differences between experimental and theoretical values suggest, however, that the invalidation effect of the oxide layers is not complete. Certainly, the activation process also has a strongly erratic component forming randomly privileged electrical pathways, thus making the process non-uniform and deviating from the proposed model. Despite these differences, and according to the measured and predicted values shown in **Figures 9** and **10**, it can be concluded that the model can be considered satisfactorily validated.

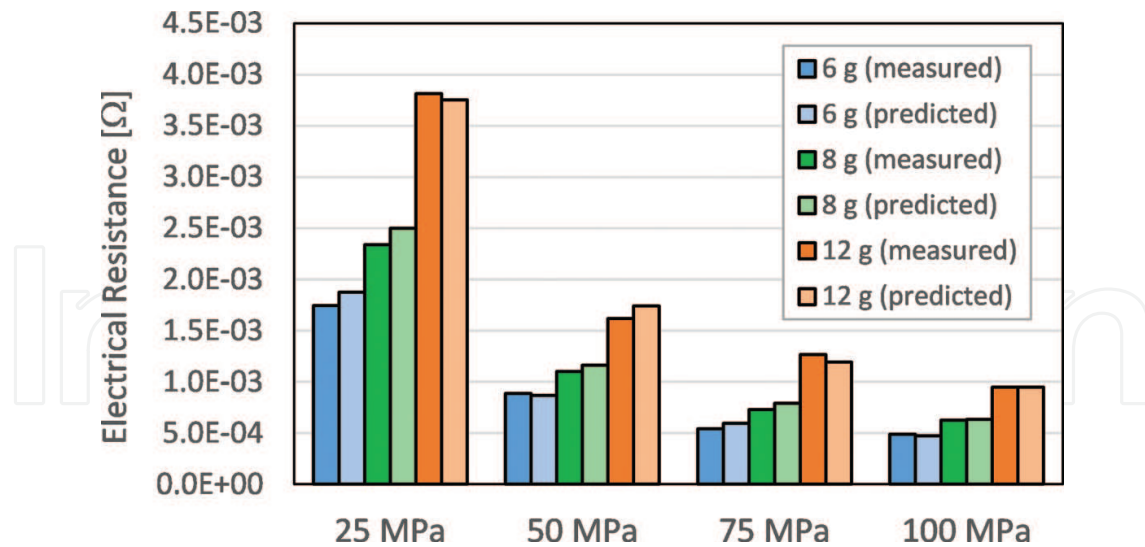


Figure 10. Measured and predicted resistance values for Fe powder columns under different pressures and masses and with a previous activation stage.

4. Conclusions

Two new equations to calculate the effective electrical resistivity of metal powder systems under pressure (constituted by oxide-free or oxide-coated metallic particles) have been developed. According to these equations, the effective electrical resistivity can be expressed as a function of the material resistivity, the porosity degree of the sample and the tap porosity of the starting powders. The latter parameter is considered a fitting parameter in the model, to be determined with initial experiences. To model powder aggregates of oxide-coated particles, two fitting parameters describing the powder descaling phenomenon are also necessary: the residual resistivity and the exponent value. This descaling phenomenon must be considered in the model to explain that resistivity does not tend to the bulk metal value if extrapolated to zero porosity and to justify the greater rate of reduction in resistivity by decreasing porosity (as compared to the case of oxide-free particles). However, both equations are formally similar from a mathematical point of view.

The validity of these equations has been experimentally tested, using sintered compacts (similar to oxide-free powder system) and powder aggregates (similar to oxide-coated powder system) of aluminum, bronze, iron and nickel with different porosity degrees. The agreement between experimental and fitted theoretical values is quite good.

The proposed equations are suitable to describe the early stages of electrical consolidation techniques. The efficiency of the electrical activation process (which causes the dielectric breakdown of the oxide layers) has been tested and interpreted on the basis of the equations presented here. The results obtained confirm the goodness of the proposed models.

Acknowledgements

Financial support of the Ministerio de Economía, Industria y Competitividad (Spain) and Feder (EU) through the research projects DPI2015-69550-C2-1-P and DPI2015-69550-C2-2-P is gratefully acknowledged. The authors also wish to thank the technicians J. Pinto, M. Madrid and M. Sánchez (University of Seville, Spain) for their experimental assistance.

Author details

Juan Manuel Montes¹, Francisco Gómez Cuevas², Jesús Cintas¹, Fátima Ternero^{1*} and Eduardo Sánchez Caballero¹

*Address all correspondence to: fternero@us.es

1 Metallurgy and Materials Science and Engineering Group, Escuela Técnica Superior de Ingeniería, Universidad de Sevilla, Sevilla, Spain

2 Department of Chemical Engineering, Physical Chemistry and Materials Science, Escuela Técnica Superior de Ingeniería, Universidad de Huelva, Huelva, Spain

References

- [1] Maxwell JC. A Treatise on Electricity and Magnetism. New York: Dover Publications Inc.; 1998 (reprinted)
- [2] Rayleigh L. On the influence of obstacles arranged in a rectangular order upon the properties of medium. The London, Edinburgh, and Dublin Philosophical Magazine and Journal of Science. 1892;**34**:481-502
- [3] Einstein A. Eine neue Bestimmung der Moleküldimensionen. Annals of Physics. 1906;**19**: 289-306
- [4] Fricke H. A mathematical treatment of the electric conductivity and capacity of dispersed systems. Physical Review Journals. 1924;**24**:575-587
- [5] Loeb AL. Thermal conductivity: III, a theory of thermal conductivity of porous materials. Journal of the American Ceramic Society. 1954;**37**(2):96-99
- [6] Murabayashi M, Takahashi Y, Mukaibo T. Effect of porosity on the thermal conductivity of ThO₂. Journal of Nuclear Science and Technology. 1969;**6**(11):657-662
- [7] Aivazov MI, Domashnev IA. Influence of porosity on the conductivity of hot-pressed titanium nitride specimens. Poroshkovaya Metallurgiya. 1968;**9**(69):51-54

- [8] Meyer R. The measurement of electrical resistivity to characterize a sintered product. *Powder Metallurgy International*. 1972;**4**(2):63-67
- [9] Schulz B. Thermal conductivity of porous and highly porous materials. *High Temperatures-High Pressures*. 1981;**13**:649-660
- [10] McLachlan DS. Equation for the conductivity of metal – Insulator mixtures. *Journal of Physics C: Solid State Physics*. 1986;**19**:1339-1345
- [11] Montes JM, Rodríguez JA, Herrera EJ. Thermal and electrical conductivities of sintered powder compacts. *Powder Metallurgy*. 2003;**46**(3):251-256
- [12] Montes JM, Cuevas FG, Cintas J. Porosity effect on the electrical conductivity of sintered powder compacts. *Applied Physics A: Materials Science & Processing*. 2008;**92**:375-380
- [13] Montes JM, Cuevas FG, Cintas J, Gallardo JM. Electrical conductivity of metal powder aggregates and sintered compacts. *Journal of Materials Science*. 2016;**51**:822-835
- [14] Garino TJ. Electrical behavior of oxidized metal powders during and after compaction. *Journal of Materials Research*. 2002;**17**(10):2691-2697
- [15] Lefebvre LP, Pleizier G, Deslandes Y. Electrical resistivity of green powder compacts. *Powder Metallurgy*. 2001;**44**(3):259-266
- [16] Cheng-Feng LI, Shen-Gang ZHU. Apparent electrical conductivity of porous titanium prepared by the powder metallurgy method. *Chinese Physics Letters*. 2005;**22**(10):2647-22650
- [17] MPIF. Standard 46, Determination of Tap Density of Metal Powders. Princeton: MPIF; 2002
- [18] Montes JM, Cintas J, Rodríguez JA, Herrera EJ. Effective pressure on powders under uniaxial compression. *Journal of Materials Science Letters*. 2003;**22**:1669-1671
- [19] Montes JM, Cuevas FG, Cintas J. A new expression for the effective pressure on powders under compression. *Computational Materials Sciences*. 2006;**36**:329-337
- [20] Montes JM, Cuevas FG, Cintas J. Effective area in powder compacts under uniaxial compression. *Materials Science and Engineering A*. 2005;**395**:208-213
- [21] Montes JM, Cuevas FG, Cintas J, Rodríguez JA, Herrera EJ. The equivalent simple cubic system in trends. In: *Materials Science Research*. New York: Nova Publishers; 2005. pp. 157-190
- [22] German RM. *Particle Packing Characteristics*. Princeton: MPIF; 1989
- [23] Efron AL. *Physics and Geometry of Disorder. Percolation Theory*. Moscow: MIR; 1985
- [24] Stauffer D, Aharony A. *Introduction to Percolation Theory*. London: Taylor and Francis; 1994

- [25] Torquato S. *Random Heterogeneous Materials: Microstructure and Macroscopic Properties*. New York: Springer; 2009
- [26] Sahimi M. *Heterogeneous Materials I*. New York: Springer; 2003
- [27] Tsuda N, Nasu K, Fujimori A, Siratori K. *Electronic Conduction in Oxides*. 2nd ed. Berlin: Springer-Verlag; 2000
- [28] Euler KJ. The conductivity of compressed powders. A review. *Journal of Power Sources*. 1978;**3**:117-136
- [29] Secondi J. Modeling powder compaction from a pressure–density law to continuum mechanics. *Powder Metallurgy*. 2002;**45**(3):213-217
- [30] Brandes EA (editor). *Smithells Metals Reference Book* (6th edition). United Kingdom: Butterworths; 1983
- [31] Li WT, McKenzie DR, McFall WD, Zhang QCH, Wiszniewski W. Breakdown mechanism of Al₂O₃ based metal-to-metal antifuses. *Solid State Electronics*. 2000;**44**:1557-1562
- [32] Drobny VF, Pulfrey DL. Properties of reactively-sputtered copper oxide thin films. *Thin Solid Films*. 1979;**61**:89-98
- [33] Akl AA. Optical properties of crystalline and non-crystalline iron oxide thin films deposited by spray pyrolysis. *Applied Surface Science*. 2004;**221**:319-329
- [34] Guziewicz M, Grochowski J, Borysiewicz M, Kaminska E, Domagala JZ, Rzodkiewicz W, Witkowski BS, Golaszewska K, Kruszka R, Ekielski M, Piotrowska A. Electrical and optical properties of NiO films deposited by magnetron sputtering. *Optica Applicata*. 2011;**XLI**(2):431-440
- [35] Huntz AM, Andrieux M, Molins R. Relation between the oxidation mechanism of nickel, the microstructure and mechanical resistance of NiO films and the nickel purity. II. Mechanical resistance of NiO films. *Materials Science and Engineering: A*. 2006;**417**:8-15
- [36] MPIF. *Standard 45, Determination of Compressibility of Metal Powders*. Princeton: MPIF; 2002